CrossMark

Multifunctional properties of microwave assisted CdO–NiO–ZnO mixed metal oxide nanocomposite: enhanced photocatalytic and antibacterial activities

K. Karthik[1] · S. Dhanuskodi[1] · C. Gobinath[3] · S. Prabukumar[2] · S. Sivaramakrishnan[2]

Abstract
A facile approach for the preparation of CdO–NiO–ZnO mixed metal oxide nanocomposite was demonstrated by microwave assisted method and characterized by XRD, SEM with EDS and FTIR. XRD exhibits CdO (cubic), NiO (cubic), ZnO (hexagonal) structure with an average crystallite size of 37, 23 and 20 nm respectively. The lattice strain and the dislocation density are evaluated by W–H method. SEM and TEM images reveal the morphology as sheet like structure and FTIR indicates the characteristic stretching frequency as Cd–O ($687 \, cm^{-1}$), Ni–O ($865 \, cm^{-1}$) and Zn–O ($472 \, cm^{-1}$). From the UV–Vis spectra, the bandgap is estimated as 2.75 eV. The fluorescence spectrum shows the emission of blue–violet (455 nm), green (524 nm) and red (678 nm). The prepared nanocomposite acts as an excellent photocatalyst for the removal of methylene blue dye under sun light irradiation. Furthermore, the antibacterial activity for concentrations (25, 50, 75 and 100 µg/mL) was carried out in-vitro against gram negative (G − Ve) i.e. *Escherichia coli, Pseudomonas aeruginosa, proteus mirablis, Aeromonas hydrophila, Salmonella typhi* and *Vibrio cholerae*; gram positive bacteria (G + Ve): *Staphylococcus aureus, Rhodococcus rhodochrous and Bacillus subtilis*. Confocal laser scanning microscopy confirms the rupture of the bacterial cell wall.

1 Introduction

Environmental pollution is one of the challenging phenomena due to rapid unregulated industrial growth over the globe. The heterocyclic dyes [Methylene blue (MB) and Rhodamine B (RB)] has wide industrial applications and harm the environment (global warming and climate change), aquatic life and also human (skin diseases, respiratory infections and chronic effects) because of its high toxicity. Till now, removal or separation of MB and RB from water has been done. The degradation of industrial effluents is very difficult using conventional methods. Alternatively, photocatalysis is one of effective methods to remove the organic pollutants from waste water [1]. Mixed metal oxide nanocomposite can be act as a suitable photocatalytic agent.

There has been an increase in the number of diseases due to bacterial transmission either by interpersonal or through contaminated surfaces. Microorganisms such as *Escherichia coli* and *S*taphylococcus *epidermis* are bacterial pathogens in hospital environments that could be acquired even from an inanimate object [2]. Enormous efforts are underway for the exploration of novel antimicrobials to combat this serious menace of antibiotic resistance. In recent era, researchers across the global are frantically looking into the exploitation of nanomaterials, primarily because of their unique properties such as high surface to volume ratio and faster chemical reactions. The antibacterial, chemical and catalytic properties of metal oxide nanocomposite make them the materials of choice for usage in sterile coatings for biomedical devices such as catheters, dental implants, adhesives, biosensors, biomaterials, tissue engineering, DNA modification, drug-delivery systems and packaging [3, 4].

Research on nanocomposite has stimulated a great interest with potential applications such as optoelectronic, photocatalytic and biological applications induced by quantum-size effect. These composites can be a variety of combinations as dielectric/dielectric, dielectric/metal,

✉ S. Dhanuskodi
   dhanus2k3@yahoo.com

1   School of Physics, Bharathidasan University, Tiruchirappalli, Tamilnadu 620 024, India

2   Department of Biotechnology and Genetic Engineering, Bharathidasan University, Tiruchirappali, Tamilnadu 620 024, India

3   Academic Body of Agriculture and Food Biotechnology, Universidad Autonoma del Estado de Hidalgo Tulancingo, 43600 Hidalgo, CP, Mexico

dielectric/semiconductor, semiconductor/semiconductor etc. Metal oxide nanocomposites are more stable and largely used in biocides and disinfectants and they have longer life than organic-based materials [5].

Zinc oxide (n-type 3.32 eV, hexagonal, exciton binding energy 60 meV) is bio safe, biocompatible and has attracted a great interest due to its unique properties and a wide applications such as transparent electronics, piezoelectric, chemical and biological sensing and catalytic reactions. Furthermore, ZnO is strongly resistant to microorganisms and it contains environmentally safe mineral (Zn) essential to humans. It has superior durability, less toxicity, greater selectivity and heat resistance [6]. Nickel oxide (NiO) has a wide range of applications as a p-type semiconductor (cubic, 3.5 eV). NiO nanostructures have been widely studied during the last few years because of its useful electronic and magnetic properties. It finds applications in gas sensing, lithium-ion battery and electrochemical capacitor [7]. Cadmium oxide (CdO) is an n-type semiconductor (cubic, 2.5 eV). It has a high electrical conductivity and optical transmission in the visible region. It has potential applications (flat panel display, organic light emitting diodes, optoelectronic devices and gas sensors) [8]. These three metal oxides have been largely used in the same applications (Photocatalysis and Biomedical). Developing a new composite material by combining the metal oxides and given a new direction of research for optoelectronic, photocatalysis and biological applications.

In nanomaterials, oxygen deficiency and surface area are the most important parameters in many applications such as gas and humidity sensing, photocatalytic degradation and antibacterial activities. As ZnO NPs has low oxygen deficiency and surface area, it can be used as an efficient gas and humidity sensor. To overcome this drawback, Sharma et al. have fabricated bimetallic ZnO–CdO composite in which CdO with high oxygen vacancies shows maximum sensitivity of 24 ppm for ethanol gas [9]. ZnO:SiO_2 composite having high surface area (462 m^2/g) senses the relative humidity (RH) with a quick response (15 s) and recovery time (16 s) in the 11–98% RH range [10]. Several reports are available for trimetallic nanocomposites which show enhanced dye degradation.

Abdus Subhan et al. have investigated the excitation wavelength dependent luminescence for $La_2O_2Co_3$.CuO. ZnO, Co_3O_4.CeO_2.ZnO and $La_2O_2Co_3$.CeO_2.ZnO nanocomposites. The photocatalytic degradation efficiency is 93.75% for the $La_2O_2Co_3$.CeO_2.ZnO composite against methyl violet 6b (MV). NiO.CeO_2.ZnO composite exhibits 96.07% efficiency for the same dye and it is also an effective antimicrobial agent against pathogenic bacteria such as *P. mirabilis* (zone of inhibition (ZOI) 15 mm). The antimicrobial activity of Ag_2O.CeO_2.ZnO against *K. Pneumoniae* shows a ZOI of 15 mm and the photocatalytic degradation efficiency against

MV is 84.04% [11–15]. Juma et al. have reported the synthesis and characterization of CuO–NiO–ZnO mixed metal oxide nanocomposite [16]. The present study reports the photocatalytic and antibacterial activities of the microwave assisted nanocomposite.

2 Materials and methods

2.1 Preparation of nanocomposite

1 M of Cd(CH_3COO)$_2$.$2H_2O$, Ni(CH_3COO)$_2$.$4H_2O$, Zn(CH_3COO)$_2$.$2H_2O$ and 2 M of NaOH were prepared in double distilled water. Solutions of Cd(CH_3COO)$_2$.$2H_2O$ and Ni(CH_3COO)$_2$.$4H_2O$ were mixed and subjected to constant stirring for 30 min at 303 K. Then the solutions of Zn(CH_3COO)$_2$.$2H_2O$ and NaOH were added to the above solution, stirred for 1 h at 303 K and irradiated for 30 min in a domestic microwave oven (2.45 GHz, 750 W) in the convection mode. The precipitate was washed thoroughly with double distilled water and ethanol and again irradiated for 15 min resulting with a solid powder. It was calcined at 673 K for 2 h to obtain nanocomposite.

2.2 Instrumentation

The synthesized compound was identified using XRD on a Riagu Mini Flexell Desktop Diffractometer (CuK_α, λ = 1.5406 Å). The morphology was examined by SEM on VEGA 3 TESCAN SEM and TEM on JEOL JEM − 2100 respectively. The molecular structure was confirmed by JASCO 460 plus FT-IR spectrometer by KBr pellet method in the range of 400–4000 cm^{-1}. The linear optical absorption characteristics were recorded using a Perkin Elmer Lambda 25 spectrophotometer and the luminescence was analysed by Fluoromax 4 spectrophotometer. Electrochemical behaviour was studied using the EG and G Park model potentiostat comprising three electrode system with the working electrode Ag/AgCl, saturated KCl as the reference electrode and a platinum wire as the counter electrode.

2.3 Photocatalytic activity

Photocatalytic activity of nanocomposite was evaluated by studying the photodegradation of methylene blue (MB) dye solution under sunlight irradiation. 2.5 mg of the prepared nanocomposite was added to a quartz photoreactor containing 100 mL of a 1 mg/L MB aqueous solution. After stirring in dark (2 h), the mixture was irradiated in sunlight with the intensity fluctuation of 950 ± 25 W m^{-2}. The residual MB in the aqueous solution was analyzed by checking the absorbance at 664 nm in the UV–Vis absorption spectra. Further, the samples were collected at regular

intervals (for every 15 min) to determine the percentage of the degradation of MB. The collected samples were filtered and centrifuged to remove the undissolved particles in the sample and the UV–Vis spectrum was recorded. The degradation percentage of the dye in the presence and absence of nanocomposite is calculated from the following equation

$$\eta = \left[(C_o - C_t) / C_o \right] \times 100\% \qquad (1)$$

η is the percentage of degradation, C_o is the initial concentration of the dye (mg/L) and C_t is the concentration of the dye after irradiation in the selected time interval (mg/L).

2.4 Antibacterial assay

The antibacterial activity of nanocomposite was tested against both the gram positive and the gram negative bacteria. Clinical isolates of *Bacillus subtilis, Staphylococcus aureus, E.coli, Salmonella typhi, Pseudomonas aeruginosa, Rhodococcus rhodochrous, proteus mirablis, Aeromonas hydrophila and Vibrio cholerae* were sub-cultured in nutrient broth for 24 h at 310 K. This study was carried out in agar by well diffusion method. nanocomposite was mixed (1 mg/mL) with sterile distilled water and loaded onto the well at the concentrations between 25 and 100 µg/mL. For positive control, standard antibiotic chloramphenicol (5 mg/mL) was used. These doses were selected based on the preliminary data obtained from earlier studies. After 24 h of incubation at 310 K, the zone of inhibition (ZOI) was measured.

2.5 Confocal laser scanning microscopy

Confocal microscopic (Carl ZEISS, LSM 710) studies were performed on a confocal laser scanning microscope (CLSM) utilizing an argon laser $\lambda = 488$ nm. Vibrio cholerae and Rhodococcus rhodochrous cultures were labelled with Acridine orange (AO) and Ethidium bromide (EB) dyes. AO and EB were used to determine the relative proportion of live and dead cells as EB specifically stains only for dead bacteria. nanocomposite (5 µg/mL) was added to the overnight grown bacterial cultures and were incubated at 310 K for 30 min in dark. 1 mL from broth of these bacterial strain cultures were harvested by centrifuging at 2500 rpm for 5 min. The pellet was resuspended in 1 mL PBS buffer. Staining was performed by adding 1 µg/mL of AO and EB. This solution was incubated for 3 h at 310 K. Likewise controls of both bacterial strains (*Vibrio cholerae* and *Rhodococcus rhodochrous*) were grown under similar conditions. A few drops of the above prepared samples were then placed on a glass slide and mounted with a cover slip and the cells were examined under the confocal laser scanning microscope.

3 Results and discussion

3.1 Structural studies

XRD pattern of nanocomposite confirms the phases cubic CdO, cubic NiO and hexagonal ZnO (Fig. 1). The diffraction peaks are well matched with the standard JCPDS Card No: 05-0640 (CdO), 89-7130 (NiO) and 65-3411 (ZnO).

The average crystallite size (D) is calculated using Debye–Scherrer's formula

$$D = k\lambda \, / \, \beta \, \cos\theta \qquad (2)$$

where k is the shape constant (0.9), λ is the wavelength of X-ray (1.5406 Å), β is the full width at half maximum (FWHM) and θ is the glancing angle.

Williamson–Hall method (W–H) suggests a way to calculate the microstrain of the prepared nanocomposite. Modified Scherrer equation is expressed as

$$\beta \, \cos\theta = (k \, \lambda \, / \, D) + (4\varepsilon \sin\theta) \qquad (3)$$

The W–H plot is expected to be horizontal line, parallel to the sinθ axis, whereas in the presence of strain, it has a non-zero slope (Fig. 2). The dislocation density strongly influences many of the properties of materials [17]. Dislocation density (δ) is calculated using the equation,

$$\delta = 1/D^2 \qquad (4)$$

The evaluated lattice parameters, crystallite size, strain and dislocation density are reported in Table 1.

3.2 Morphological studies

Figure 3a show typical SEM images of prepared nanocomposite which indicate the formation of sheet like structure.
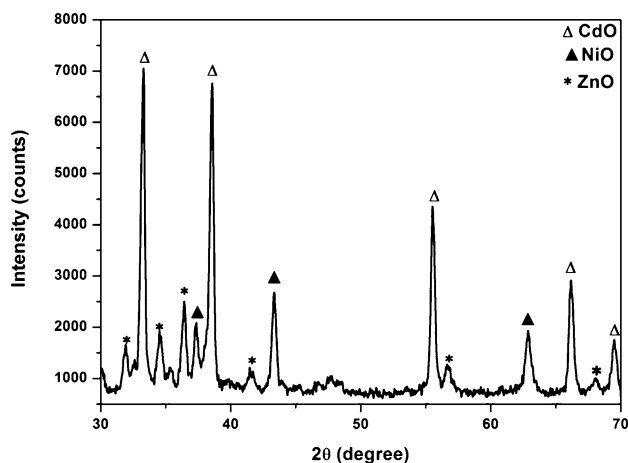

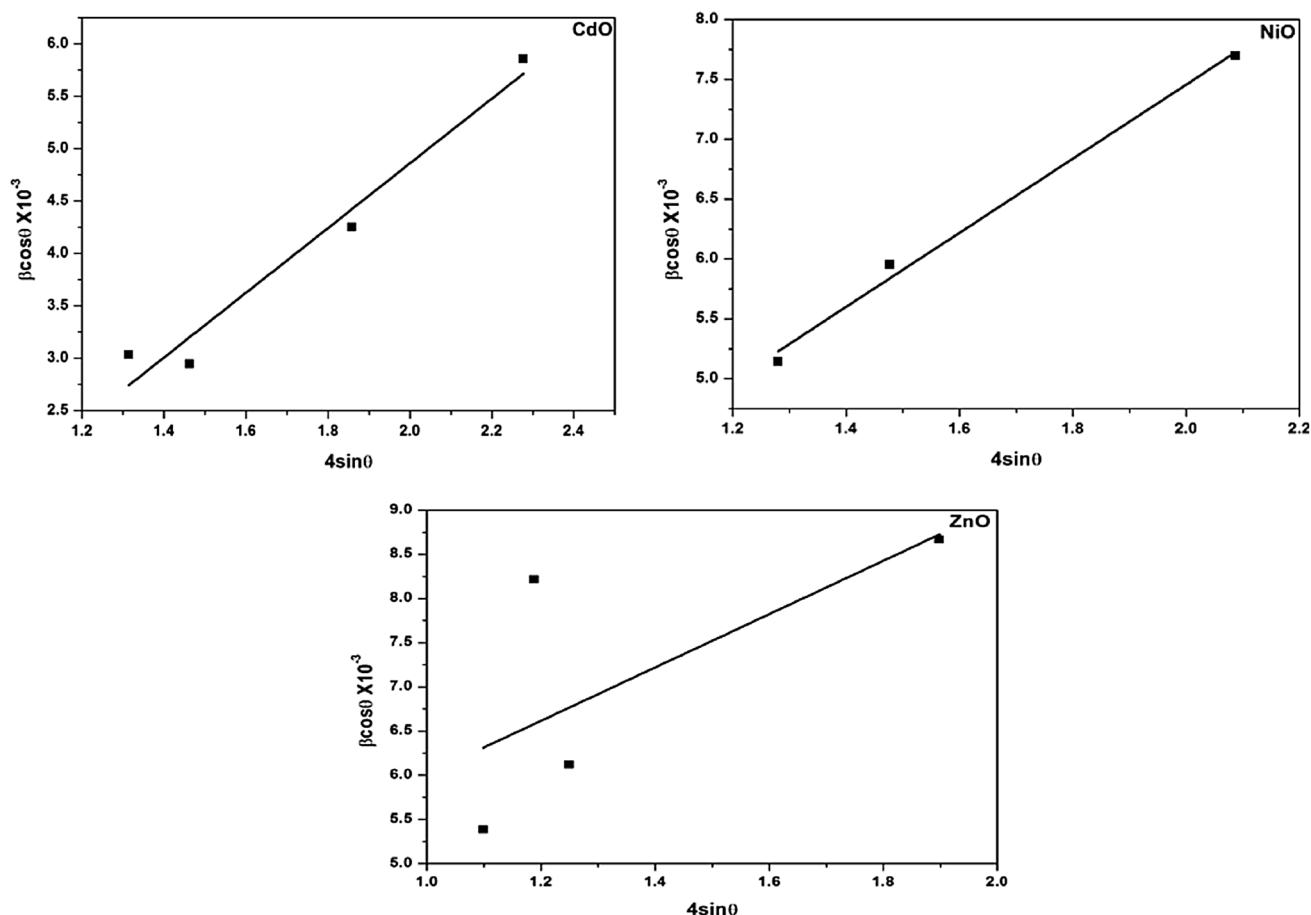**Fig. 1** XRD pattern of mixed metal oxide nanocomposite

Fig. 2 Williamson–Hall plot of mixed metal oxide nanocomposite

Table 1 Structural parameters of nanocomposite

Sample	Phase	Lattice parameters		Crystallite size D (nm)	Strain (ε) $\times 10^{-3}$	Dislocation density (δ) $\times 10^{14}$ (lines/ m^2)
		a (Å)	c (Å)			
CdO–NiO–ZnO	CdO	4.6759	–	37	36.96	1.091
	NiO	4.1717	–	23	22.77	2.092
	ZnO	3.2370	5.1844	20	20.34	2.795

TEM image clearly shows the sheet like structure (Fig. 3b). Figure 3c shows the average size of the nanosheets is 139 nm. The EDS is displayed in Fig. 3d, with a separate peak of Cd (19.59%), Ni (12.72%), Zn (3.98%) and O (63.71%).

3.3 FTIR study

Strong peaks at 687, 865 and 472 cm^{-1} are due to the characteristic metallic bonding of Cd–O, Ni–O and Zn–O respectively. The peak at 1449 cm^{-1} is attributed to bending vibrational mode of CH$_3$ and the peak at 2469 cm^{-1} is ascribed to stretching carbonyl group of O–C–O vibrations. Stretching and bending vibrational modes of hydroxyl groups are observed at 3319 and 1649 cm^{-1} (Fig. 4). The observed hydroxyl group is the supplementary evidence for the reported generation of hydroxyl radicals which play an important role in the enhancement of antibacterial activity of the prepared nanocomposite [18].
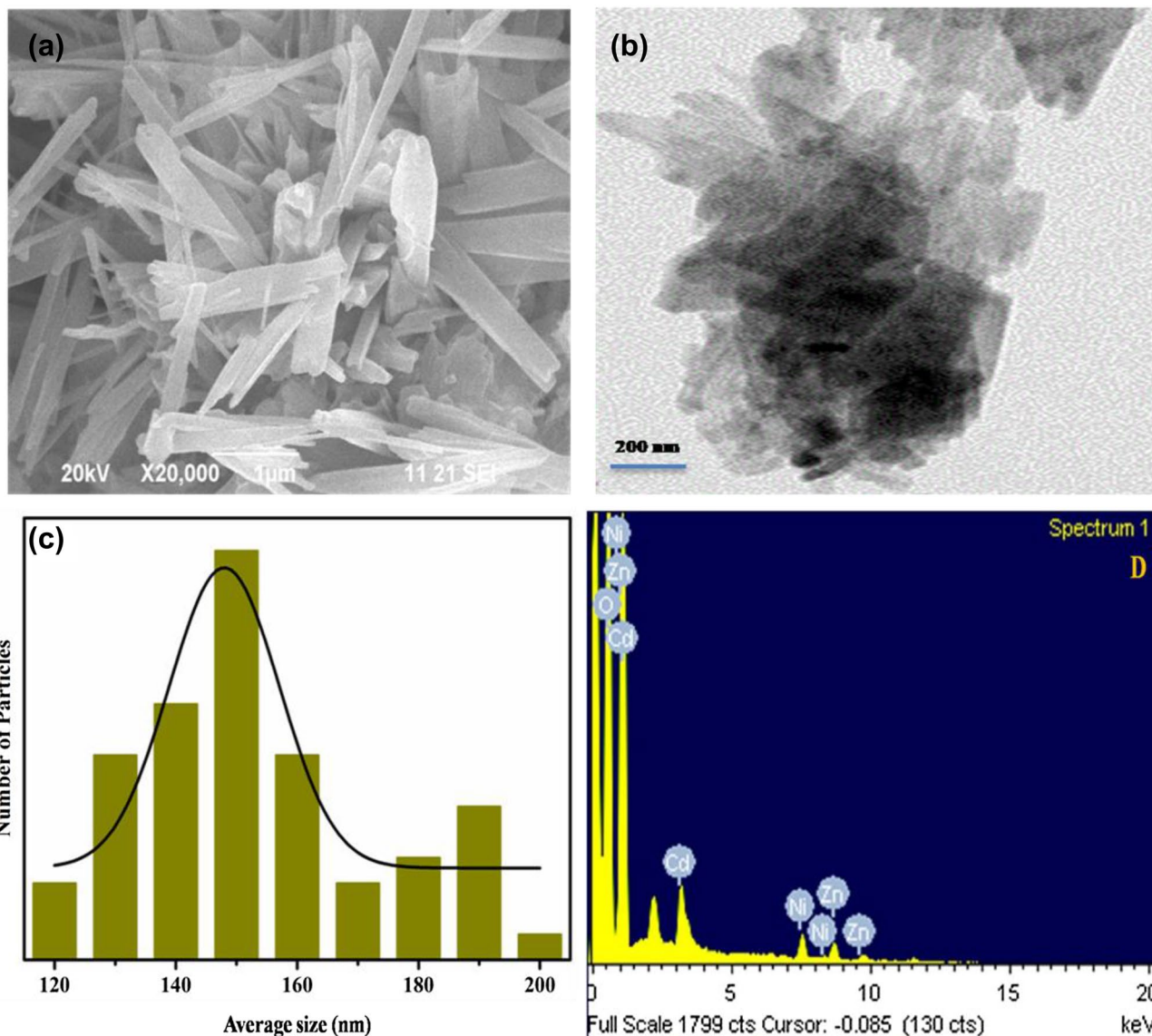
Fig. 3 **a** SEM. **b** TEM. **c** Particle size distribution. **d** EDS images of mixed metal oxide nanocomposite

4 Optical properties

4.1 Linear optical studies

The optical absorption edge is observed at 216 nm (CdO), 379 nm (NiO) and 250 nm (ZnO) due to the scattering from the individual oxide phases (Fig. 5a). The corresponding energy band gap spectrum is calculated from Tauc's relation.

$$\alpha h\nu = A\,(h\nu - E_g)^n \tag{5}$$

where A is the characteristics parameter (free of photon energy) for this transition, h is the Planck's constant, ν is the frequency of light and E_g is the optical energy bandgap.
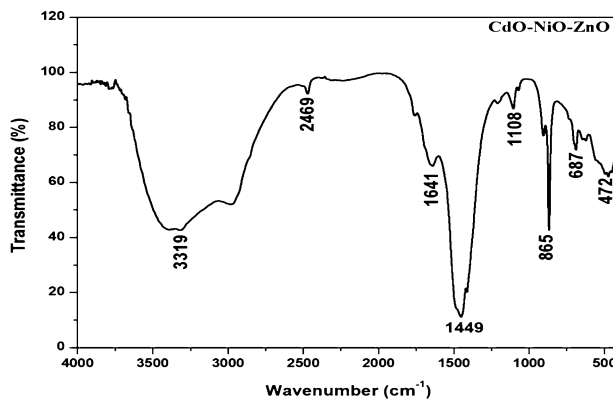

Fig. 4 FTIR spectra of mixed metal oxide nanocomposite

The parameter n characterizes the transition process involved and takes the value 2 for direct allowed transition and ½ for indirect allowed transition. The plot of $(\alpha h\upsilon)^2$ vs $h\upsilon$ is shown in Fig. 5b, from which the optical energy bandgap (E_g) is estimated as 2.75 eV by extrapolating the linear part up to zero on the energy axis. This optical bandgap lies between that of CdO (2.5 eV), NiO (3.6 eV) and ZnO (3.37 eV). Therefore, bandgap is tuning the volume fractions of the suitable for several applications such as photovoltaics, photocatalysis and thermoelectrics.

4.2 Luminescence studies

Figure 6 shows the room temperature luminescence spectrum at an excitation wavelength of 220 nm. A strong peak at 455 nm (2.72 eV) reveals the generation of .OH radicals. Generally H^+, $\cdot OH$ and H_2O_2 are the main active species responsible to damage the DNA, cell membranes and cellular proteins that lead to the microbes death. It is well known that UV emission peak originates from the recombination of free excitons through an exciton–exciton collision process corresponding to the near band edge

(NBE) emission of the wide band gap of metal oxide. The luminescence spectrum exhibits emission at 360, 372 and 524 nm which is attributed to the near band edge emission of ZnO, NiO and CdO respectively. The emission at 490 nm corresponds to the blue emission. However, a weak visible emission (476 nm) is assigned to the defect
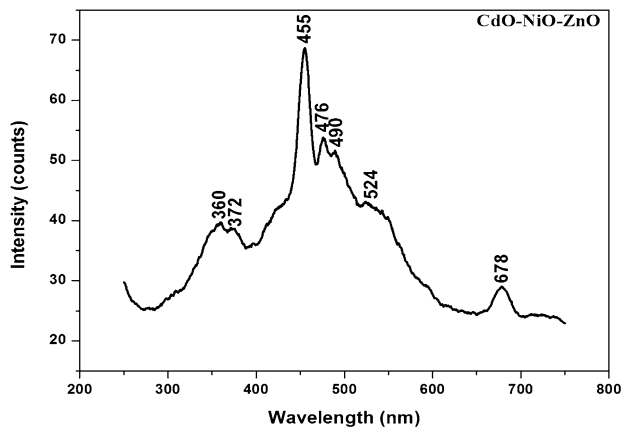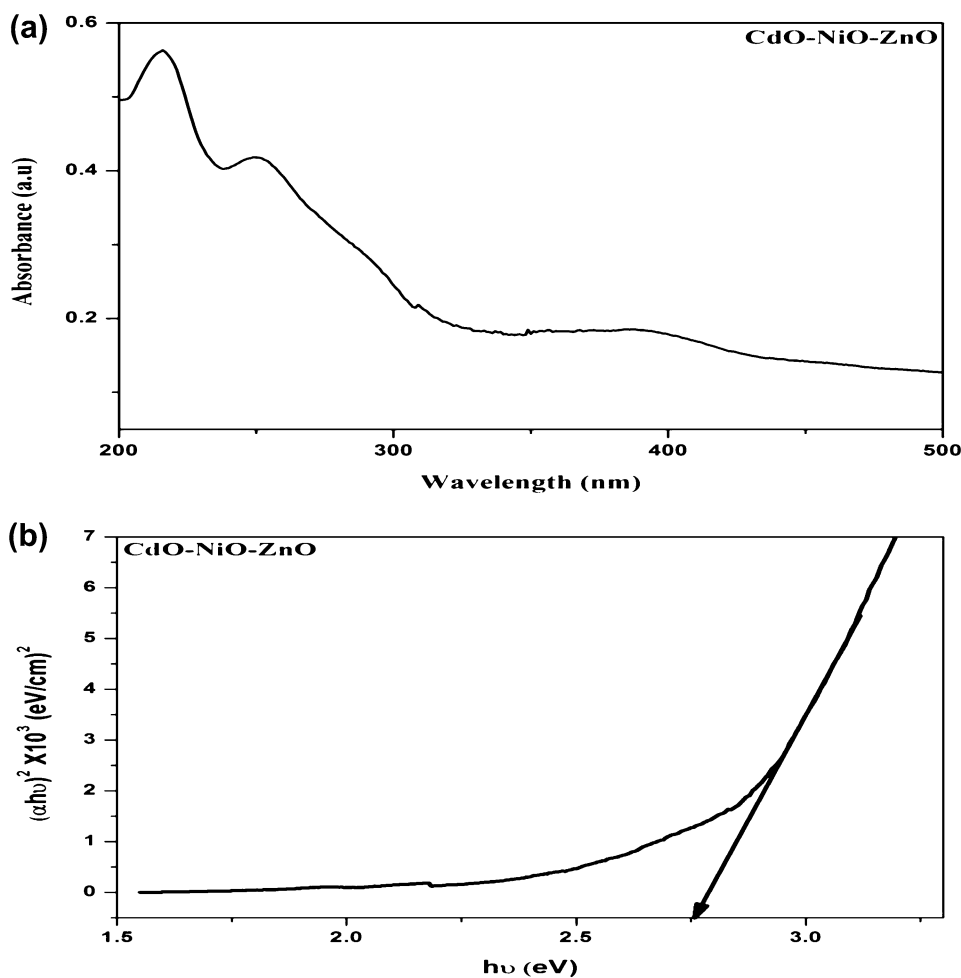

Fig. 6 Luminescence spectrum of mixed metal oxide nanocomposite

Fig. 5 a UV–Vis absorption. **b** Optical energy bandgap of mixed metal oxide nanocomposite

levels within the bandgap of NiO, associated with the oxygen vacancies or Ni interstitials. In general, NiO exhibits three types of charge states of oxygen vacancies, such as namely neutral oxygen vacancy (V_o^o), singly ionized oxygen vacancy (V_o^+) and doubly ionized oxygen vacancy (V_o^{++}). The oxygen vacancies are located below the bottom of the conduction band (CB) in the sequence of V_o^o, V_o^+ and V_o^{++}, from the top to bottom. The red emission centred at 628 nm is attributed to transition from zinc interstitial (Zn_i) to oxygen interstitial (O_i) defect levels in ZnO. These defects are probably on the crystal surfaces, causing faster and more effective trapping of photo generated holes at the surface site. nanocomposite is a promising candidate for luminescent, nanophotonics, optoelectronic and biological fluorescence labelling applications [19, 20].

4.3 Electrochemical studies

Electrochemical study was analysed for nanocomposite in dimethyl formamide solution under nitrogen atmosphere in the potential range of $+1.5$ to -1.5 V. Tetra butyl ammonium perchlorate (TBAP) (0.05 M) was used as the supporting electrolyte. The one electron nature of reduction has been confirmed by comparing its current height with that of a standard ferrocene–ferrocenium couple under identical experimental conditions. The redox potentials are virtually independent of scan rates, indicating quasi-reversibility [21].

There is a distinct pair of irreversible reduction peaks during the anodic and cathodic sweeps (Fig. 7). The electrochemical parameter (half wave potential, $E_{1/2} = 95$ mV) is calculated using the equation.

$$E_{1/2} = \frac{1}{2}\left(Ep_c - Ep_a\right) \tag{6}$$

where Ep_c (-0.65 V) and Ep_a (-0.84 V) are the potentials at cathodic and anodic peaks. The separation between the two peak potentials, ΔE_p (in volts).

$$\Delta E_p = \left(Ep_a - Ep_c\right) \tag{7}$$

The calculated electrochemical parameter ΔE_p is 0.19 V.

4.4 Photocatalytic activity

The efficiency of the CdO–NiO–ZnO nanocomposite was evaluated against the MB dye degradation under sun light irradiation. The degradation of MB dye solution ($\lambda = 664$ nm) was monitored using UV visible spectrometer as shown in Fig. 8a. Under sun light irradiation, the main
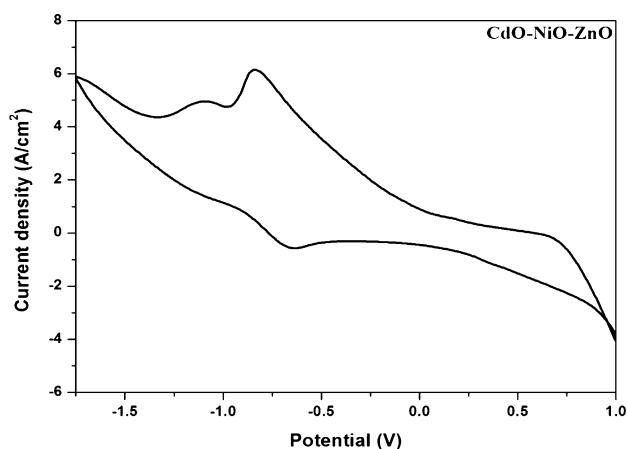

Fig. 7 Cyclic voltammogram of mixed metal oxide nanocomposite

absorption peak of MB was gradually decreased in the presence of CdO–NiO–ZnO nanocomposite. The completed degradation of MB dye solution was achieved within 90 min.

The prepared CdO–NiO–ZnO nanocomposite showed good activity due to the unique morphology, effective charge separation and crystalline nature. The photocatalytic performance of CdO–NiO–ZnO nanocomposite was demonstrated by kinetic studies and the decomposition was followed pseudo-first order kinetic equation

$$C_t = C_0 e^{-Kt} \tag{8}$$

Alternatively

$$\ln\left(C_0/C_t\right) = Kt \tag{9}$$

where C and C_0 are the concentration of the dye solution at different time intervals t and initial concentration at $t = o$ min. K is the first order rate constant. The rate constant of CdO–NiO–ZnO nanocomposite is 0.0180 min^{-1} for the degradation of the MB dye. The present photocatalytic degradation efficiency is compared with some metal oxide nanocomposite against MB dye (Table 2).

4.5 Photodegradation mechanism

Mechanism for the degradation of dye solution was expressed in the following equations
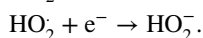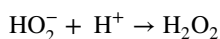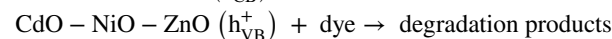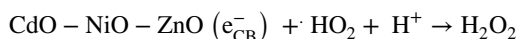
$$CdO - NiO - ZnO + h\nu \rightarrow CdO - NiO - ZnO\left(e_{CB}^- + h_{VB}^+\right)$$
$$CdO - NiO - ZnO\left(e_{CB}^-\right) + O_2 \rightarrow CdO - NiO - ZnO + O_2$$
$$H_2O \rightarrow H^+ + OH^{\cdot}$$
$${}^{\cdot}O_2 + H^- \rightarrow {}^{\cdot}HO_2$$
$$CdO - NiO - ZnO\left(e_{CB}^-\right) + {}^{\cdot}HO_2 + H^+ \rightarrow H_2O_2$$
$$CdO - NiO - ZnO\left(h_{VB}^+\right) + dye \rightarrow degradation\ products$$
$$HO_2^- + H^+ \rightarrow H_2O_2$$
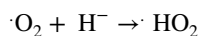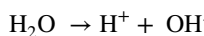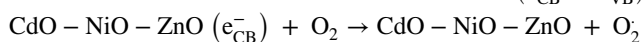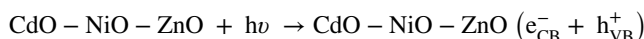$$HO_2 + e^- \rightarrow HO_2^-.$$

Fig. 8 a Time dependent absorption spectra. **b** Schematic diagram of mechanism of photo degradation of MB dye of CdO–NiO–ZnO mixed metal oxide nanocomposite
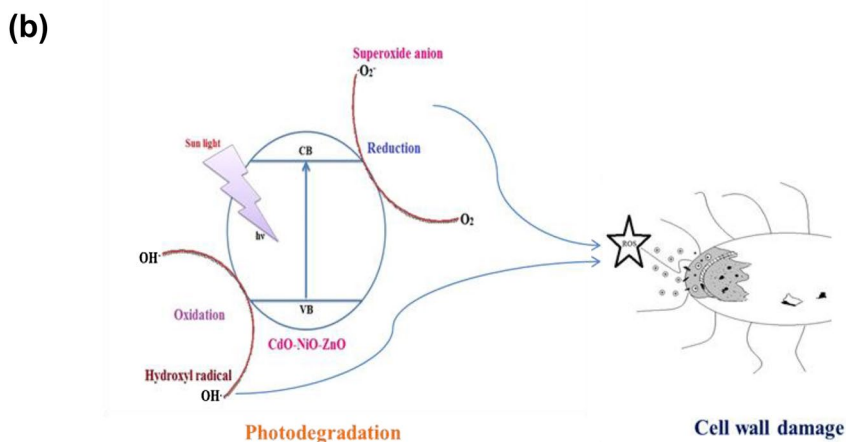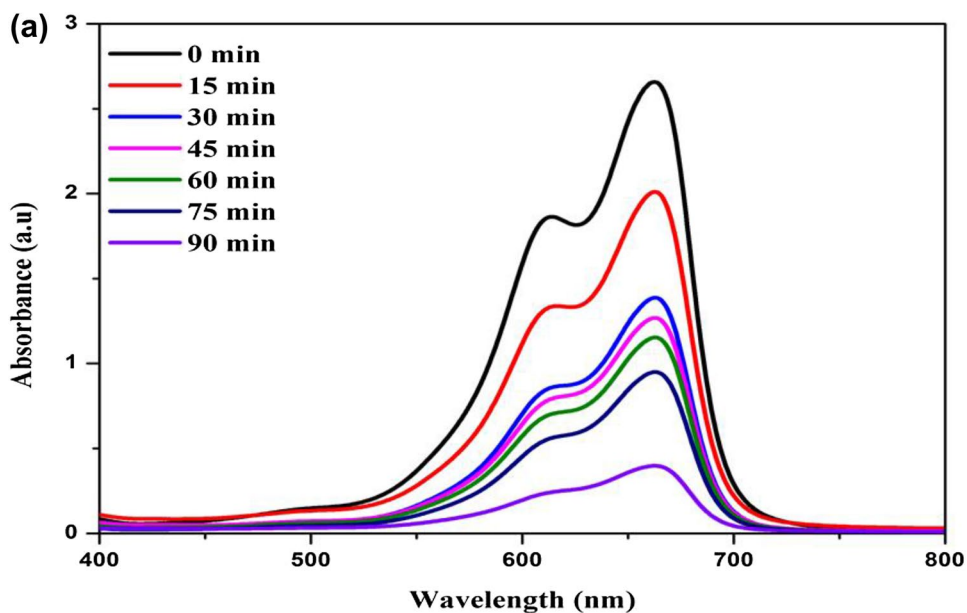

Table 2 Comparison of photocatalytic activity of some metal oxide nanocomposites against methylene blue

Sample	Degradation efficiency (%)	References
ZnO/CeO$_2$ (50:50)	64.6	[38]
ZnO/CeO$_2$ (80:20)	74.3	[38]
CdO–NiO	78.0	[39]
Fe$_3$O$_4$/CuO/ZnO	79.0	[40]
ZnO/grapheme/TiO$_2$	82.8	[41]
CdO–NiO–ZnO	89.0	Present work

CdO–NiO–ZnO nanocomposite is illuminated under the sunlight radiation which leads to the formation e$^-$ in the conduction band and h$^+$ in the valance band. As the photo generated electrons are transfer to the conduction band and valance band. The electron reacts with molecular oxygen to produce less toxic super oxide anion radical (O$_2$.) through a reductive process. The hole in the valance band can attract electrons from water or hydroxyl ions to generate most reactive hydroxyl radical (.OH) through an oxidative process. The superoxide anions react with electron–hole pairs and generate H$_2$O$_2$. The negatively charged hydroxyl radical (.OH$^-$) and super oxide radicals (.O$_2$). The combination of metal oxide generates more active catalytic centres which facilitate the photodegradation performance (Fig. 8b) [22–26].

4.6 Antibacterial studies

The antibacterial activity was performed against the gram-positive bacteria (*Bacillus subtilis, Staphylococcus aureus and Rhodococcus rhodochrous*) and the gram-negative bacteria (*E.coli, Salmonella typhi, Pseudomonas aeruginosa, proteus mirablis, Aeromonas hydrophila and Vibrio cholerae*). The concentration of nanocomposite is varied between
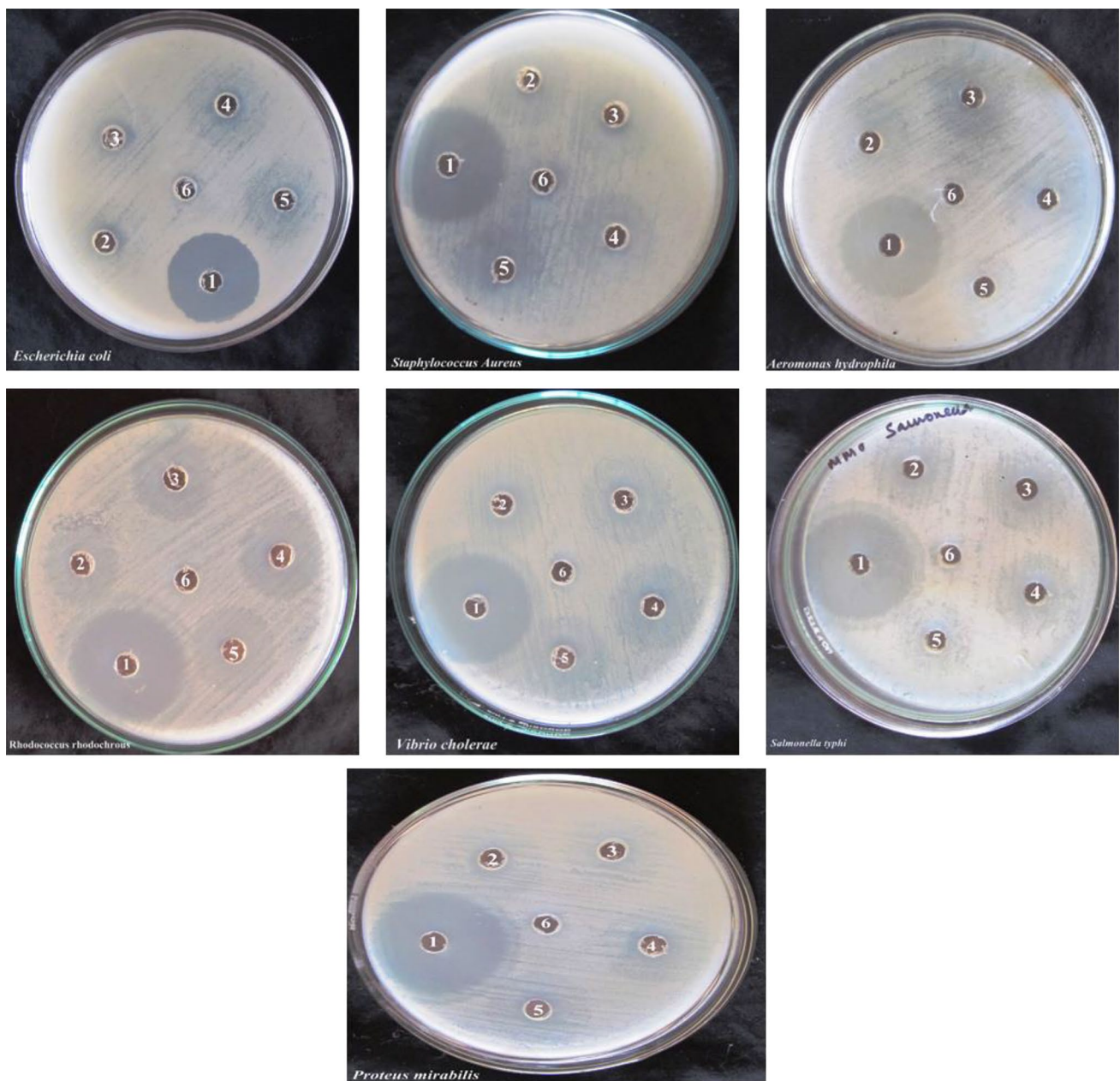
Fig. 9 Antibacterial activity of CdO–NiO–ZnO mixed metal oxide nanocomposite against Gram-positive and Gram-negative bacterium *E.coli, Staphylococcus aureus, Aeromonas hydrophila, Rhodococcus rhodochrous, Vibrio cholerae, Salmonella typhi* and *Proteus mirab-lis*—(1) standard antibiotics, (2) CdO–NiO–ZnO nanocomposite 25 μg/mL, (3) CdO–NiO–ZnO nanocomposite 50 μg/mL, (4) CdO–NiO–ZnO nanocomposite 75 μg/mL, (5) CdO–NiO–ZnO nanocomposite 100 μg/mL and (6) distilled water (negative control)

25 and 100 μg/mL (Fig. 9). The most significant effect of nanocomposite is found for the concentration (100 μg/mL) per disc against *Vibrio cholerae* to produce a 27 mm inhibition zone of gram-negative bacteria. The zone of inhibition (ZOI) of other human pathogens is presented in Table 3.

It is well known that if the diameter of antibacterial inhibition zone is higher than 6 mm, the sample has better antibacterial activity. However, if the diameter of antibacterial inhibition zone is equal to or less than 6 mm, the

sample has poorer antibacterial activity. From the results in Tables 3 and 4, it is seen that the nanocomposite has better antibacterial activity because the antibacterial inhibition zone is much larger than 6 mm for all the tested bacterial strain.

In particular, many studies have been reported for photogeneration of reactive oxygen species (ROS) on the surface of metal-oxide nanocomposites as suggested by Angel Ezhilarasi et al. [27]. ROS such as super oxide anions ($.O_2^-$)

Table 3 Antimicrobial activity of CdO–NiO–ZnO nanocomposite at concentrations (25, 50, 75, 100 µg/mL)

Tested bacteria	Gram reaction	Zone of inhibition (mm)				Positive control	Negative control
		25	50	75	100		
P. aeruginosa	− ve	20	22	24	25	30	–
S. aureus	+ ve	18	21	25	27	31	–
E.coli	− ve	10	12	14	16	27	–
Proteus mirabilis	− ve	19	22	24	26	33	–
Aeromonas	− ve	17	20	22	24	28	
B. subtilis	+ ve	16	19	21	24	33	–
Vibrio cholera	− ve	16	22	25	27	33	–
Rhodococcus	+ ve	22	23	25	25	33	
S. typhi	− ve	15	20	24	26	32	–
Antibacterial index		17.0	20.11	22.67	24.44	31.11	**–**

cannot penetrate into cell membrane, but they cause damage to the nucleic acids, lipids and DNA. Among the ROS, hydrogen peroxide (H_2O_2) and hydroxyl radical (.OH) are more powerful oxidizing agents. They directly penetrate into the cell membrane of the bacteria and cause injuries and prevent the growth of the cells.

A higher ROS value generally depends on a larger surface area, appropriate crystallite size, increase of oxygen vacancies and the facillation of diffusion and mass transportion of reactant molecules. From the XRD results, the average crystallite size is found to be 27 nm leading to higher antibacterial activity. From the photoluminescence studies, the red emission at 678 nm indicates the ionized oxygen defect. Electrochemical half wave potential of nanocomposite

Table 4 Comparison of antibacterial activity for selected human pathogens

Bacteria	Materials	Zone of inhibition (mm)	References
S. aureus	NiO.CeO2. ZnO	14	[13]
	Ag_2O. CeO2. ZnO	11	[15]
	CdS–ZnO	22	[42]
	ZnO:Cu/graphene	16	[43]
	CdO–NiO–ZnO	27	Present work
E. coli	NiO.CeO2. ZnO	11	[13]
	Ag_2O. CeO2. ZnO	12	[15]
	CdS-ZnO	14	[42]
	ZnO:Cu/graphene	16	[43]
	CdO–NiO–ZnO	16	Present work
Proteus mirabilis	NiO.CeO2. ZnO	15	[13]
	Ag_2O. CeO2. ZnO	12	[15]
	CdO–NiO–ZnO	26	Present work
P. aeruginosa	NiO.CeO2. ZnO	13	[13]
	Ag_2O. CeO2. ZnO	11	[15]
	CdO–NiO–ZnO	25	Present work

(0.19 V) is optimum potential to penetrate the cell wall membrane and causes the severe damage.

Other mechanisms are also involved in the antibacterial activity. Nanocomposite interferes with the bacteria cell membrane and bind with mesosome. There is a perturbation in the mesosome functions of cellular respiration, DNA replication cell division and thereby the surface area of bacterial cell membrane is increased. These intracellular functional changes introduce the oxidative stress induced by ROS generation due to the cell expiry. Considering the above facts, a schematic picture is shown in (Fig. 10). When the heavy metal ions Cd^{2+}, Ni^{2+} and Zn^{2+} released by nanocomposite surface come into contact with the cell membranes of the microbe, the cell membranes with negative charge and Cd^{2+}, Ni^{2+} and Zn^{2+} with positive charge mutually attract, and the Cd^{2+}, Ni^{2+} and Zn^{2+} penetrates into the cell membrane and react with the thiol groups (– SH) of the proteins present on the bactericidal cell surface. The nanomaterials inactivate the proteins and decrease the membrane permeability leading to the death of the microbe.

The metal oxide with uneven surface texture due to rough edges and corners contribute to the mechanical damage of the cell membranes. From the SEM image, it is clear that the nanocomposite has uneven ridges at the outer surface which influence the antibacterial activity. The combination of various factors such as size, surface defects play an important role in the toxicological behaviour of nanocomposite. Interestingly, in the present study, nanocomposite concentration of 100 µg/mL is more prominent in cell inhibition *Vibrio cholerae* (27 mm) and also the inhibition of all the other tested bacteria are comparable to standard antibiotics (Chloramphenicol) and is compared in Table 3. CdO–NiO–ZnO nanocomposite exhibits more ZOI against *Staphylococcus aureus, E.coli, Pseudomonas aeruginosa, proteus mirablis* and it is compared with some other metal oxide nanocomposites
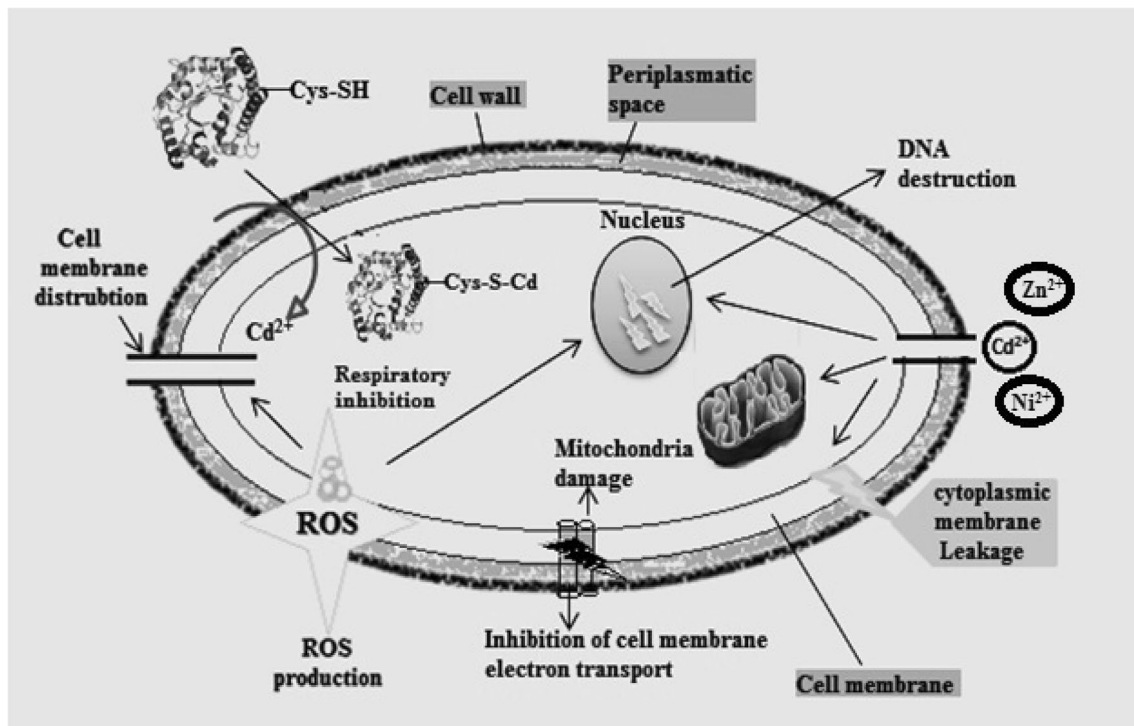
Fig. 10 Mechanism of antibacterial activity of mixed metal oxide nanocomposite

(Table 4). Therefore fabrication of nanocomposites and characterization for biomedical applications are possible in near future [28–35].

4.7 Confocal microscopy studies

To prove the effect of nanocomposite on the viability of *Vibrio cholerae* and *Rhodococcus rhodochrous* strains, confocal microscopy was performed using CLSM. Biological strains were stained with AO and EB with the addition of nanocomposite. A control stained with the AO and EB was also prepared for comparison (Fig. 11). From the AO and EB binding to the double stranded nucleic acids, it is confirmed that the nanocomposite damages the bacterial cell wall. The untreated cells show green fluorescence due to their viable or live cells indicating intact cell wall structure and the red fluorescence is the characteristics of the dead cells (treated cells). These results suggest that the treatment of *Vibrio cholerae* and *Rhodococcus rhodochrous* strains with

nanocomposite leads to the cell death or bacteriostatic effect [36, 37].

5 Conclusion

In the present study, nanocomposite was synthesized by the microwave-assisted route. SEM and TEM image shows the nanosheets like structure and the presence of Cd, Ni, Zn and O is confirmed by EDAX analysis. The FTIR spectrum represents the characteristic vibrational modes of Cd–O, Ni–O and Zn–O. The optical bandgap is 2.75 eV from UV–Vis absorption spectrum; while the luminescence spectrum shows an emission of blue, violet and red light useful in optoelectronics applications. The prepared CdO–NiO–ZnO nanocomposite proved an effective photocatalyst for the decolourisation of MB dye under sun light. Nanocomposite inhibits the growth of various microorganisms markedly, exhibiting higher antimicrobial activity against both Gram-positive and Gram-negative bacteria.
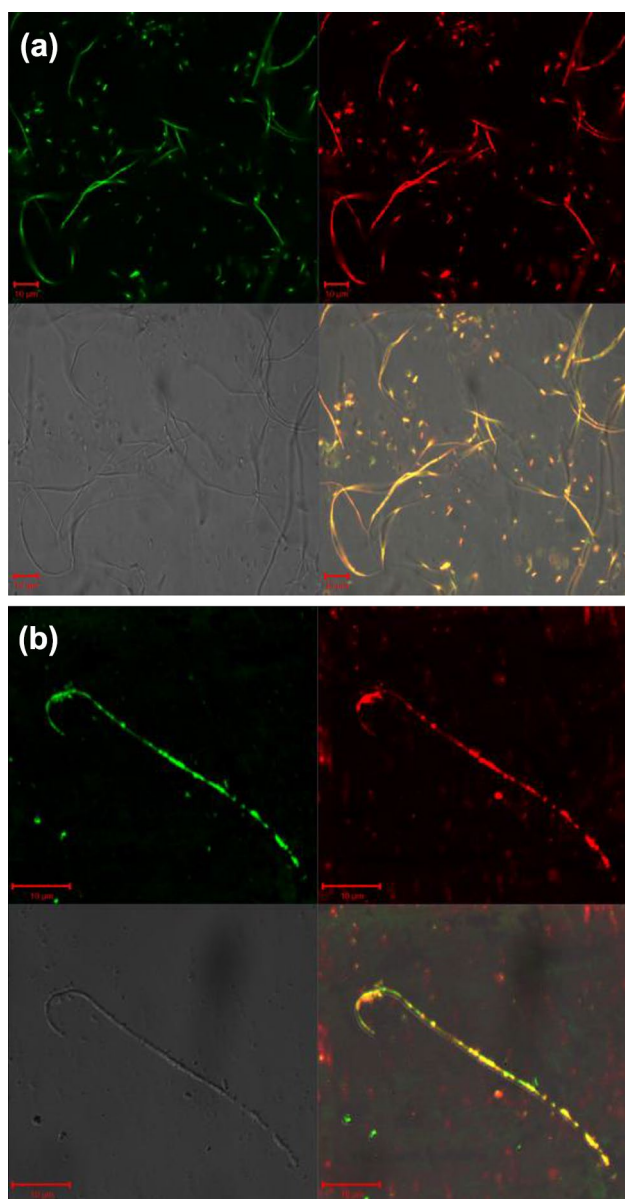
Fig. 11 CLSM images of **a** *Vibrio cholerae* and **b** *Rhodococcus rhodochrous*

References

1. S. Amreetha, S. Dhanuskodi, A. Nithya, K. Jothivenkatachalam, Three way electron transfer of C–N–S tri doped two phase junction of TiO_2 nanoparticles for efficient visible light photocatalytic dye degradation. RSC Adv **6**, 7854 (2016)

2. B.R. Cruz-Ortiz, D.A. Cortes-Hernadez, M.L. Diaz-Jimenez, J. E. Mauricio-Benarides, Antibacterial activity of TiO_2–$CaSiTiO_5$ materials synthesized from a spent catalyst. Ceram. Int **41**, 2484 (2015)***

3. S. Velho-Pereira, A. Noronha, A. Mathias, R. Zakane, V. Naik, P. Naik, A.X. Salker, S.R. Naik, Antibacterial action of doped $CoFe_2O_4$ nanocrystals on multidrug resistant bacterial strains. Mater. Sci. Eng. C **52**, 282 (2015)

4. A. Ishita Matai, P. Sachdev, S. Dubey, B. Uday Kumar, P. Bhushan, Gopinath, Antibacterial activity and mechanism of Ag–ZnO nanocomposite on *S. aureus* and GFP expressing antibiotic resistant *E. Coli*. Colloids Surf. B: Biointerfaces **115**, 359 (2014)

5. R. Joyce Stella, G. Thirumala Rao, B. Babu, V. Pushpa Manjari, Ch..V. Reddy, J. Shim, R. V. S. S. N. Ravikumar, A facial synthesis and spectral characterization of Cu^{2+} doped CdO/ZnS nanocomposite. J. Magn. Magn. Mater **384**, 6 (2014)

6. K. Raja, P.S. Ramesh, D. Geetha, Synthesis, structural and optical properties of ZnO and Ni doped ZnO hexagonal nanorods by co-precipitation method, Spectrochimic. Acta Part A Mol. Biomol. Spectrosc **120**, 19 (2014)

7. F.C.W. Zhou, H. Yao, P. Fan, J. Yang, Z. Fei, M. Zhong, Self-assembly of NiO nanoparticles in lignin-derived mesoporous carbons for supercapacitor applications. Green Chem **15**, 3057 (2013)

8. B. Sahin, Y. Gulen, F. Bayansal, H.A. Centinkara, H.S. Guder, Structural and optical properties Ba doped CdO films prepared by SILAR method. Superlattices Microstruct **65**, 56 (2014)

9. K. Sharma, S.S. Dotdar, K.S. Pakhare, B.M. Sargar, M.V. Rokade, N.L. Tarwal, The selective ethanol gas sensing performance of $CdO_{1-X}ZnO_X$ nanocomposite. J. Mater. Sci: Mater. Electron. (2016). https://doi.org/10.1007/S10854-016-5984-1

10. V.K. Tomer, S. Duhan, S. Sharma, R. Malik, S.P. Nehra, S. Devi, One pot synthesis of mesoporous ZnO–SiO_2 nanocomposite as high performance humidity sensor. Colloids Surf. A. Physicochem. Eng. Asp **483**, 121 (2015)

11. M.A. Subhan, T. Ahmed, N. Uddin, Synthesis, structure, PL and photocatalytic activities of $La_2O_2CO_3.CeO_2.ZnO$ fabricated by co-precipitation method, Spectrochimic. Acta Part A: Mol. Biomol. Spectrosc **138**, 827 (2015)

12. M.A. Subhan, T. Ahmed, Synthesis, characterization and spectroscopy investigations of novel nano multi-metal oxide $Co_3O_4.CeO_2.ZnO$, Spectrochimic. Acta Part A: Mol. Biomol. Spectrosc **129**, 377 (2014)

13. M.A. Subhan, T. Ahmed, N. Uddin, A.K. Azad, K. Begum, Synthesis, characterization, PL properties, photocatalytic and antibacterial activities of nano multi-metal oxide $NiO.CeO_2.ZnO$, Spectrochimic. Acta Part A. Mol. Biomol. Spectrosc **136**, 824 (2015)

14. M.A. Subhan, T. Ahmed, M.R. Awal, A.M.M. Fahim, Synthesis, structure and excitation wavelength dependent PL properties of novel nanocomposite $La_2O_2CO_3.CuO.ZnO$, Spectrochimic. Acta Part A: Mol. Biomol. Spectrosc **132**, 550 (2014)

15. M.A. Subhan, N. Uddin, P. Sarker, H. Nakata, R. Makioka, Synthesis, characterization, low temperature solid state PL and photocatalytic activities of Ag_2O, $CeO_2.ZnO$ nanocomposite, Spectrochimic. Acta Part A. Mol. Biomol. Spectrosc **151**, 56 (2015)

16. A.O. Juma, E.A. Arbab, C.M. Muiva, L.M. Lepodise, G.T. Mola, Synthesis and characterization of CuO–NiO–ZnO mixed metal oxide nanocomposite. J. Alloy. Compd **723**, 866 (2017)

17. K. Karthik, S. Dhanuskodi, Structural and optical properties of microwave assisted CdO–NiO nanocomposite, AIP Conf. Proc **1731**, 050021 (2016)

18. K.C. Lalithambika, A. Thanyumanavan, K. Ravichandran, S. Sriram, Photocatalytic and antibacterial activities of eco-friendly green synthesized ZnO and NiO nanoparticles. J. Mater. Sci. Mater. Electron **27**, 1 (2016)

19. V. Rajendran, K. Anandan, Different ionic surfactants assisted solvothermal synthesis of zero, three and one-dimensional nickel oxide nanostructures and their optical properties. Mater. Sci. Semicond. Proc **38**, 203 (2016)

20. A.T. Robert Xavier, K. Ravichandran, S. Ravichandran, D. Mantha, Ravinder, Sm doping effect on structural, morphological, luminescence and antibacterial activity of CdO nanoparticles. J. Mater. Sci: Mater. Electron **27**, 11182 (2016)

21. N.G. Tsierkezos, M. Puschner, U. Ritter, A. Knauer, L. Hafermann, J.M. Kohler, Electrochemical response of nitrogen doped multi-walled carbon nanotubes decorated with gold and iridium nanoparticles toward ferrocynaide/ferricynaide redox system. Ionics **22**, 1957 (2016)

22. G.V. Khade, M.B. Suwarnkar, N.L. Gavade, P.M. Garadkar, Sol–gel microwave assisted synthesis of Sm doped TiO_2 nanoparticles and their photocatalytic activity for the degradation of methyil orange under sunlight. J. Mater. Sci: Mater. Electron **27**, 6425 (2016)

23. S. Manikandan, K.B. Reungadevi, K. Ravichandran, P.V. Rajkumar, K. Boubaker, Enhanced photocatalytic, antibacterial and magnetic properties of ZnO nanoparticles through lattice compatible cobalt doping. J. Mater. Sci: Mater. Electron **27**, 11890 (2012)

24. G.P. Awasathi, S.P. Adhikari, S. Ko, H.J. Kim, C.H. Park, C.S. Kim, Facial synthesis of ZnO flowers modified graphene like MoS_2 sheets for enhanced visible light driven photocatalytic activity and antibacterial properties. J. Alloys Compd. **682**, 208 (2016)

25. Z. Nasira, M. Shakir, R. Wahab, M. Shoeb, P. Alam, R.H. Khan, M. Mobin, Co-precipitation synthesis and characterization of Co doped SnO_2 NPs, HSA interaction via various spectroscopic techniques and their antimicrobial and photocatalytic activities. Int. J. Biol. Mac **94**, 554 (2017)

26. S. Ragupathy, T. Sathya, Synthesis and characterization of SnO_2 loaded on groundnut shell activated carbon and photocatalytic activity on MB dye under sunlight radiation. J. Mater. Sci: Mater. Electron **27**, 5770 (2016)

27. A.A. Ezhilarasi, J.J. Vijaya, K. Kaviyarasu, M. Mazza, A. Ayeshamariam, L.J. Kennedy, Green synthesis of NiO nanoparticles using *Moringa oleifra* extract and their biomedical applications: cytotoxicity effect of nanoparticles against HT-29 cancer cells. J. Photochem. Photobiol. B Biol **164**, 352 (2016)

28. K. Karthik, S. Dhanuskodi, C. Gobinath, S. Prabukumar, S. Sivaramakrishnan, Andrographis paniculata extract mediated green synthesis of CdO nanoparticles and its electrochemical and antibacterial studies. J. Mater. Sci: Mater. Electron **28**, 7991 (2017)

29. K. Karthik, S. Dhanuskodi, C. Gopinath, S. Sivaramakrishnan, Antibacterial activities of CdO microplates synthesized by hydrothermal method. Int. J. Innov. Res. Sci. Eng. 558–561. http://ijirse. in/docs/ican14/ican105.pdf

30. K. Karthik, S. Dhanuskodi, C. Gobinath, S. Sivaramakrishnan, Microwave-assisted synthesis of CdO–ZnO nanocomposite and its antibacterial activity against human pathogens. Spectrochimic. Acta Part A. Mol. Biomol. Spectrosc **139**, 7 (2015)

31. K. Karthik, S. Dhanuskodi, C. Gobinath, S. Prabukumar, S. Sivaramakrishnan, Photocatalytic and antibacterial activities of hydrothermally prepared CdO nanoparticles. J. Mater. Sci. Mater. Electron **28**, 11420 (2017)

32. K. Karthik, S. Dhanuskodi, S. Prabukumar, C. Gobinath, S. Sivaramakrishnan, Microwave assisted green synthesis of MgO nanorods and their antibacterial and anti-breast cancer activities. Mater. Lett **206**, 217 (2017)

33. M.H.S. Poor, M. Khatami, H. Azizi, Y. Abazari, Cytotoxic activity of biosynthesized Ag nanoparticles by Plantago major towards a human breast cancer cell line. Rend. Lincei **28**, 693 (2017)

34. M. Khatami, S. Kharazi, Z. Kishani Farahani, H. Azizi, M. Augusto Lima Nobe, The anti-cancer effect of octagon and spherical silver nanoparticles on MCF-7 breast cancer cell line. Tehran Univ. Med. J. **75**, 72 (2017)

35. S.M. Mortazavi, M. Khatami, I. Sharifi, H. Heli, K. Kaykavousi, M.H.S. Poor, S. Kharazi, M.A.L. Nobre, Bacterial biosynthesis of gold nanoparticles using *Salmonella enterica* subsp. *enterica* serovar typhi isolated from blood and stool specimens of patients. J. Clust. Sci **28**, 2997 (2017)

36. K. Karthik, S. Dhanuskodi, S. Prabukumar, C. Gobinath, S. Sivaramakrishnan, Nanostructured CdO–NiO composite for multifunctional applications. J. Phys. Chem. Solids **112**, 106 (2018)

37. K. Karthik, S. Dhanuskodi, S. Prabukumar, C. Gobinath, S. Sivaramakrishnan, Dielectric and antibacterial studies of microwave assisted calcium hydroxide nanoparticles. J. Mater. Sci: Mater. Electron **28**, 16509 (2017)

38. S. Rajendran, M.M. Khan, F. Gracia, J. Qin, V.K. Gupta, S. Arumainathan, Ce^{3+} ion induced visible light photocatalytic degradation and electrochemical activity of ZnO/CeO_2 nanocomposite. Sci. Rep **6**, 31641 (2016)

39. T. Linda, S. Muthupoongodi, X. Sahaya Shajan, S. Balakumar, Fabrication and characterisation of chitosan templated CdO/NiO nanocomposite for dye degradation. Optik **127**, 8287 (2016)

40. H. Ardiansyah Taufik, R. Tju, Saleh, Enhanced UV photocatalytic performance of magnetic $Fe_3O_4/CuO/ZnO/NGP$ nanocomposites. J. Phy. Conf. Ser. **710**, 012004 (2016)

41. P. Nuengmatcha, S. Chanthai, R. Mahachai, W.-C. Oh, Sonocatalytic performance of $ZnO/graphene/TiO_2$ nanocomposite for degradation of dye pollutants (methylene blue, texbrite BAC-L, texbrite BBU-L and texbrite NFW-L) under ultrasonic irradiation. Dyes Pigm. **134**, 487 (2016)

42. T.K. Jana, S.K. Maji, A. Pal, R.P. Maiti, T.K. Dolai, K. Chatterjee, Photocatalytic and antibacterial activity of cadmium sulphide/zinc oxide nanocomposite with varied morphology. J. Colloid Interf. Sci **480**, 9 (2016)

43. K. Ravichandran, N. Chidhambaram, S. Gobalakrishnan, Copper and graphene activated ZnO nanoparticles for enhanced photocatalytic and antibacterial activities. J. Phys. Chem. Solids **93**, 82 (2016)